Brazilian Journal of Geophysics
Brazilian Geophysical Society
ISSN 2764-8044
DOI: 10.22564/brjg.v43i2.2342

GEOMECHANICAL AND GEOPRESSURE MODELING FROM SEISMIC VELOCITIES IN PELOTAS BASIN

Marcos Fetter[1], Guilherme Lenz[1], Roberto Miyamoto Pessoa[1], Ursula Belem da Silva[2],
Tais Renata Zanato[3], Rodrigo Stern[1], and Marco Cetale[1]

[1]Universidade Federal Fluminense - UFF/DOT/GISIS, Niterói, RJ, Brazil
[2]Emerson Brazil
[3]SLB Brazil

*Corresponding author: marcosfetter@id.uff.br

ABSTRACT. Most of the information available in frontier exploration areas comes from seismic data, eventually from legacy 2D seismic lines. This is the case of the Pelotas Basin, the southernmost basin along the Atlantic continental margin in Brazil. The basin belongs to the Austral sector of the rift and breakup of the Gondwana Supercon- tinent, in the Early Cretaceous. Significant hydrocarbon discoveries have been reported over the last few years in this sector, along the counterpart African margin, in ultra deep-water, offshore Namibia. This article describes a successfully tested workflow to forecast geomechanical and petroleum system information during seismic reprocessing of outdated 2D data from the Pelotas Basin. A geomechanical-geopressure model was produced from seismic velocities double-checked with both normal move out and image gathers. The model, which was computed with standard equations (eg. Gardner's and Eaton's), and conceptual velocity gradients of normal compaction trends, is fully consistent with the mechanical stratigraphy and deformation analysis of the studied area, close to the shelf border in the Central Pelotas Basin. The geomechanical results pertinent to petroleum systems indicated good seal potential and probably hydrocar- bon generation associated with an overpressure regime in the deeper Paleogene and Cretaceous successions of the basin, particularly beyond shelf border and slope. In this way, the Pelotas Basin may share, in deep-water environments, the same promising play found in recent times in Namibia.

Keywords: seismic reprocessing; velocity analysis; geopressure and geomechanic modeling; petroleum system modeling; mechanical stratigraphy

INTRODUCTION

It is common practice in the upstream O&G industry to address seismic processing, geomechanic modeling, and analysis of petroleum systems with separated teams working independently. Even considering the gain in focus, this subdivision of work can cause some delay, and possibly some loss, of relevant business information. In this work, we show an alternative integrated approach applied to an ongoing research project in the Pelotas Basin, an almost untouched exploratory frontier, in the southernmost part of the Brazilian continental margin, well known by the prolific petroleum provinces in Santos and Campos basins.

This work is part of a research effort to study the potential hydrocarbon systems of the Pelotas Basin, on the continental margin of the Austral Gondwana segment in South America, with scope for reprocessing aged seismic data with new technologies and workflows. The proposed workflow, which is based on quantitative seismic interpretation (Avseth et al., 2010; Dutta et al., 2021), can anticipate both geomechanical and petroleum system information during seismic processing. It is also suggested that the multidisciplinary approach of the methodology can compensate in part the scarcity of data in exploratory frontier areas, even in the case of reprocessing vintage seismic data, and can also add value to seismic processing deliverables.

GEOLOGICAL SETTING

The Pelotas Basin is located on the southern Brazilian continental margin in the South Atlantic (Fig. 1). It is an extensional basin that evolved to an intraplate continental margin and corresponds to the northern portion of the Austral segment of the Gondwana breakup, which occurred during the Early Cretaceous (Abreu, 1998; Fontana, 1996; Lovecchio et al., 2020).

At the Barremian-Aptian transition, the continental crust was still subject to extension and thinning in the central segment of the Gondwana breakup, to the north of the Pelotas Basin, while in the Austral segment an oceanic spreading system was already installed (Lovecchio et al., 2020). Both in South-American and African margins, the Austral segment of Gondwana rifting and break-up is still an exploratory frontier, contrasting with the above-mentioned Central segment, which encompasses some world class well established provinces, with many prolific petroleum systems in both margins. The first major hydrocarbon discoveries on the continental margins of the Austral segment are very recent (Blakeley, 2022; Hedley et al., 2022). The discoveries occurred in Namibia, along the counterpart African margin, in the transition between the Luderitz and Orange basins.

The geodynamic blueprint of the architecture of the Pelotas Basin is defined by intense magmatic activity during the syn-rift phase, in the Early Cretaceous (Abreu, 1998; Stica et al., 2014; Harkin et al., 2020; Bueno, 2021). The magmatic processes produced characteristic packages of Seaward Dipping Reflectors (SDRs) controlled by antithetic normal faults along a hinge-type flexural rift segment (Stica et al., 2014; Bueno, 2021).

The late-rift and post-rift evolution of Pelotas Basin is characterized by a second order transgressive-regressive cycle (Abreu, 1998; Bueno, 2021). The intraplate continental margin was filled with a marine sedimentary package, mostly siliciclastic. A transgressive regime was active from the Cretaceous to the Paleogene with a well defined onlap pattern. Regression started during the Eocene-Oligocene transition (**EOT**), and is still active, with a characteristic progradation pattern (Abreu, 1998; Bueno, 2021). The most expressive feature of the Neogene progradation is the Rio Grande Fan (**RGF** in Fig. 1), which is a huge sedimentary wedge deposited beyond the shelf border in southern Pelotas Basin, that hosts a world class gas hydrate accumulation (Miller et al., 2015; Bueno, 2021; Cassel et al., 2022).

So far, there are no proven active petroleum systems in the Pelotas Basin, as gas hydrates are probably biogenic (Miller et al., 2015). However, Paleocene shales with high organic carbon (TOC) were already reported (Bueno, 2021), suggesting that distal deposits associated with anoxic events of the transgressive phase are potential source rocks. Possible reservoirs include carbonates in the northern portion of the basin, and many intervals with deepwater siliciclastic sandstones along the basin. The seal potential is associated with the widespread shale successions.

The **stratigraphic framework** used in this work is mainly defined by the top of the Paleogene and by the top of the Cretaceous (Cassel et al., 2022). This framework is actually very simple and mostly easy to recognize in seismic sections (Fig. 2). The top of the Cretaceous (green horizon - 66 Ma in Fig. 2) is quite conformable, with an onlaping pattern above the Lower Cretaceous and the Basement. The top of the Ypresian (Eocene

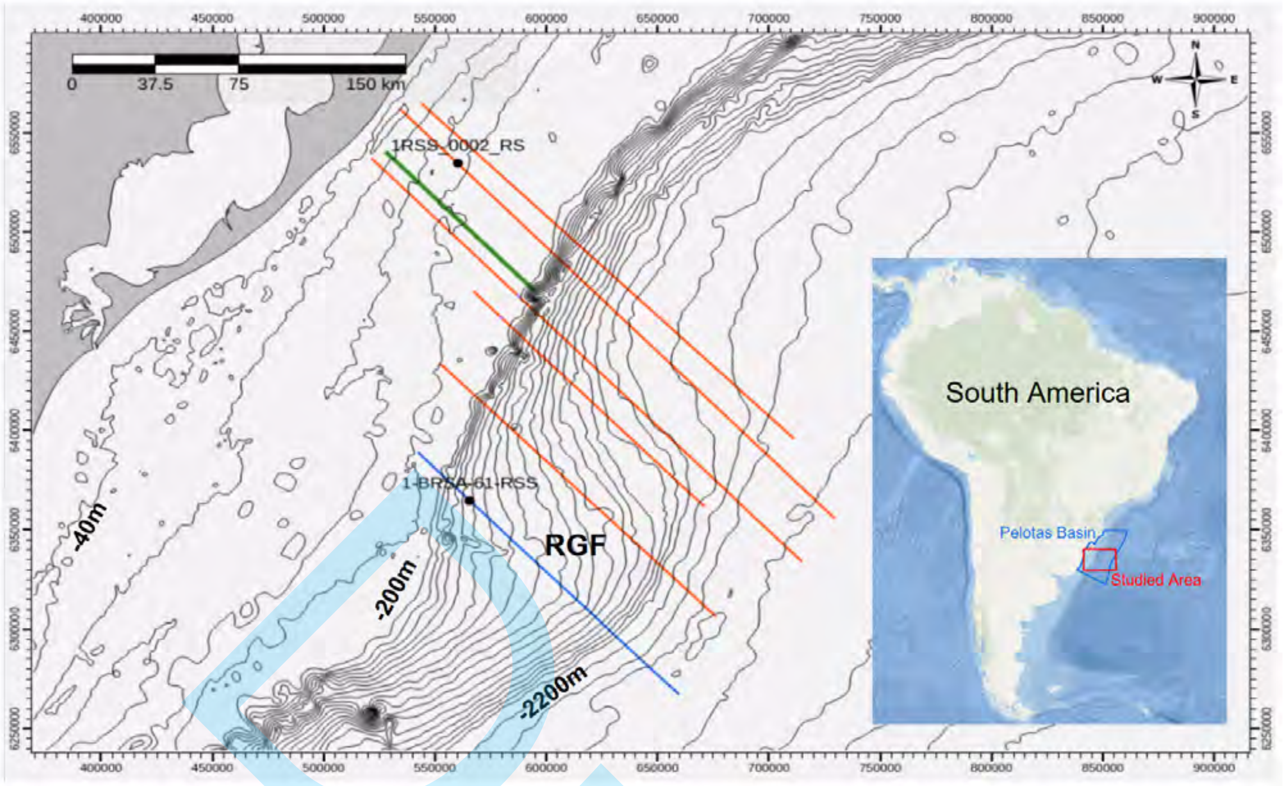

Figure 1: The studied area in the Pelotas Basin along the southernmost continental margin of Brazil. Black thin contours are the bathymetric map. Observe the bathymetric expression of the **RGF** - Rio Grande Fan sedimentary wedge, deposited during the late Neogene to Recent in distal Pelotas Basin ($area \approx 5000km^2; thickness \approx 1.5km$). Shelf border is 200 m water depth; base of the cone is 2200 m water depth. The colored straight lines indicate the position of the seismic lines used in this work. The green seismic line was used to exemplify the seismic velocity analysis (Fig. 5). The orange seismic lines were used to support the structural analysis; the well 1-RSS-0002-RS was used for stratigraphic correlation (Figs. 7, 8 and 9). The blue seismic line indicates the position of well 1-BRSA-61-RSS, terminated in the Neogene section due to overpressure problems (data from well reports provided by the Brazilian Petroleum Agency - ANP; Fig. 15).

orange horizon - 48 Ma in Fig. 2) probably represents an important punctuated lowstand during the second order transgressive cycle. The regressive cycle started at **EOT**, just below the top of the Paleogene (top of Chattian/Oligocene blue horizon - 23 Ma in Fig. 2).

DATA AND METHODS

The methodology applied in this project follows a three-step main workflow: ***(i) Velocity Analysis***, ***(ii) Structural Analysis and Geomechanical Modeling***, and ***(iii) Petroleum System Geomechanics***. The data set comprises legacy 2D pre-stack seismic lines, and two control wells in the studied area, in the Pelotas Basin (Fig. 1). The seismic and well data were provided by the Brazilian Petroleum Agency (ANP). As all steps were developed early during seismic processing, it was possible to analyze the data and results in real time.

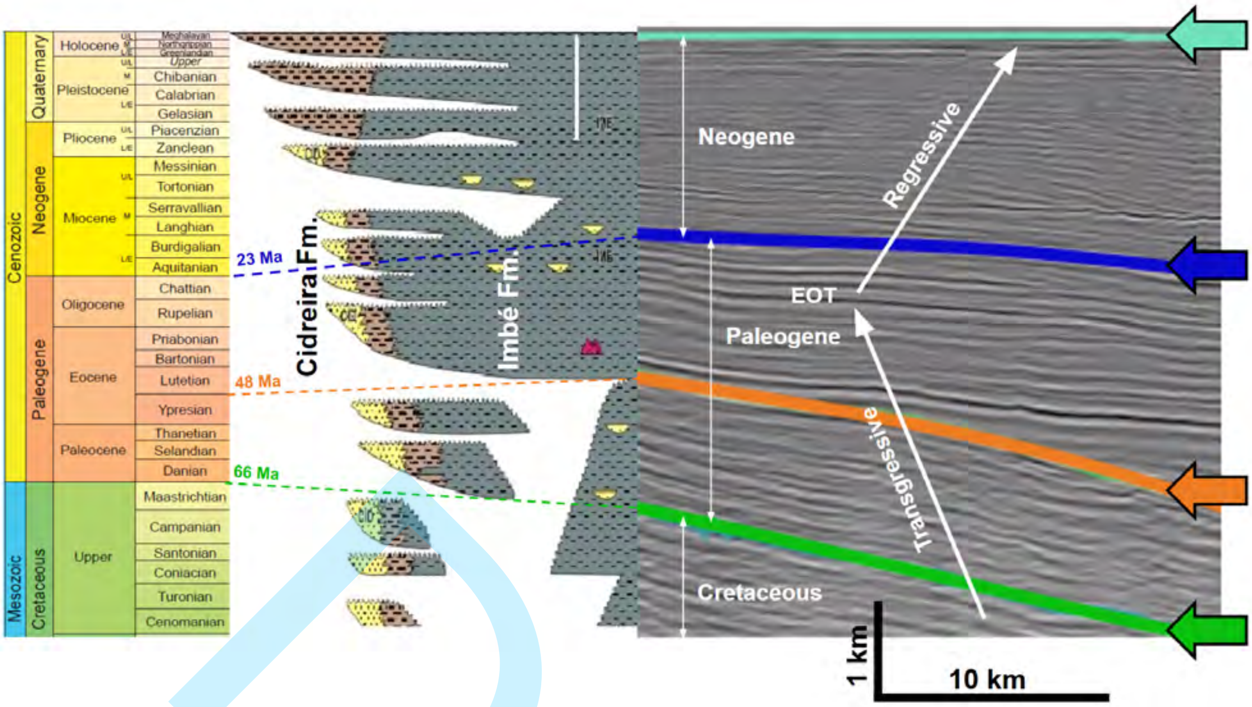

Figure 2: General **stratigraphic framework** used in this work, defined by the second order transgressive-regressive cycle that define the sedimentary filling of the **Pelotas Basin**; adapted from Bueno (2021) and Cassel et al. (2022). Sea Bottom - light green; top Chattian (Oligocene - 23 Ma) - blue; top Ypresian (Eocene - 48 Ma) - orange; top Maastrichtian (U/L Cretaceous - 66 Ma) - green. Seismic section is NW-SE oriented (NW on the left). **EOT** is the Eocene-Oligocene transition. Lithostratigraphy corresponds to the proximal Cidreira Formation (shelf sandstones and shales) and the distal Imbé Formation (deepwater shales and turbidites).

Velocity analysis

The first step of the proposed workflow is seismic velocity analysis, which is in fact a quantitative interpretation task performed early during seismic processing. To exemplify the procedures and results of seismic velocity analysis, we concentrated in three common mid-point (CMP) gathers along a seismic line acquired in the late 1960s in the Pelotas Basin (green line in Fig. 1). The reprocessed 2D line is a dip-oriented line in the central Pelotas Basin shelf, so our results and conclusions are mostly related to this proximal domain of the basin, between the coast and the shelf edge.

In seismic processing, reflections of subsurface rock interfaces in CMP gathers (Fig. 3.a) are defined by hyperbolic transit time curves according to Equation 1, were $T(x)$ is the transit time of the wave path from source to receiver, x is the source-receiver offset, V is the normal move-out velocity of wave propagation in the rock (V_{NMO}), and T_0 is the zero-offset (vertical) double transit time of the reflexion event. Stacking velocity analysis is to search, for each reflexion event in the data, the V_{NMO_i} that better fits the data for the respective $T0_i$. V_{NMO} picking is normally done with *Semblance* (energy) plots, in *velocity* × *time* domain (Fig. 3b).

$$T(x) = \sqrt{(xV)^2 + T_0^2} \tag{1}$$

$$\Delta T_{NMO} = T(x) - T_0 \tag{2}$$

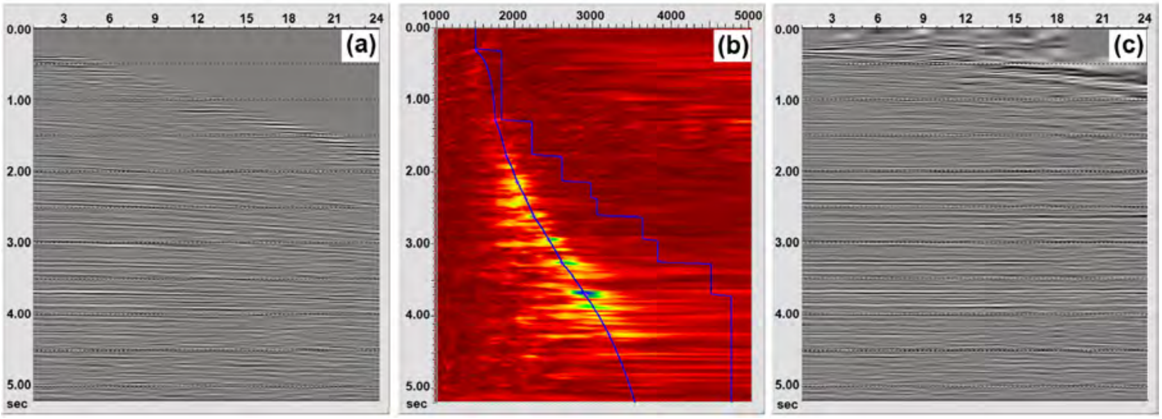

Figure 3: Velocity analysis. (a) CMP gather with reflection travel time hyperbolas. (b) Semblance plot (yellow-blue colors indicate high energy): continuous blue curve on the left corresponds to stacking velocity (V_{NMO}) picks; blue step function on the right corresponds to interval velocity (DIX V_{INT}). (c) NMO corrected CMP gather with flattened reflections.

The obtained velocity functions (T_{0i}, V_{NMOi}) are used to correct ΔT_{NMO} (Eq. 2) for the reflexion events in CMP gathers (Fig. 3). With NMO corrected CMP gathers (Fig. 3c) it's possible to stack (to sum) the data in order to obtain seismic traces and seismic sections.

Besides being used to obtain stack seismic sections in time domain, the NMO velocity, which is an approximated root mean square velocity (V_{RMS}), can be converted to interval velocity (V_{INT}) through inversion techniques, like DIX inversion (Dix, 1955). In Figure 6b, the step function is the DIX inverted V_{INT} correspondent to the picked V_{NMO} function. The interval velocity V_{INT} is used in seismic processing to obtain seismic images in depth domain, through pre-stack depth migration. It is also important to observe that V_{INT} is a rock property that can be correlated with rock facies, petrophysical properties, and geomechanical properties. In this way, velocity analysis is indeed the first approach to quantitative seismic interpretation. Interval velocities (V_{INT}) were in turn converted to average velocities (V_{AVG}), which can be used to convert seismic data and interpretation from time to depth domain (scaling).

Structural analysis, geomechanical and geopressure modeling

The next step of the workflow is the geomechanical and geopressure modeling, which take into account the seismic velocities gathered before, the stratigraphic framework (Fig. 2) and the data from the structural and deformation analysis (see detailed workflow in Fig. 4). Most of the information available for geomechanical and geopressure modeling in frontier exploration areas comes from seismic data. In this way, geomechanic and geopressure models are, in fact, an important and straightforward byproduct of velocity models, which can be obtained early during seismic processing, through standard quantitative seismic interpretation procedures.

The structural and deformation analysis is exemplified with five seismic lines oriented in a dip direction along the studied area (orange lines in Fig. 1). We used mostly the ***Continuity*** seismic attribute that enhanced the deformation pattern and its correlation with the stratigraphic framework (Fig. 2).

Geomechanical and geopressure models express the stress state in the studied formations. The main components of geomechanic models are principal stresses, pore pressures (geopressures), rock properties, and structural deformation patterns (Zoback, 2007). In this work, we used the standard equations of Gardner (Gardner et al.,

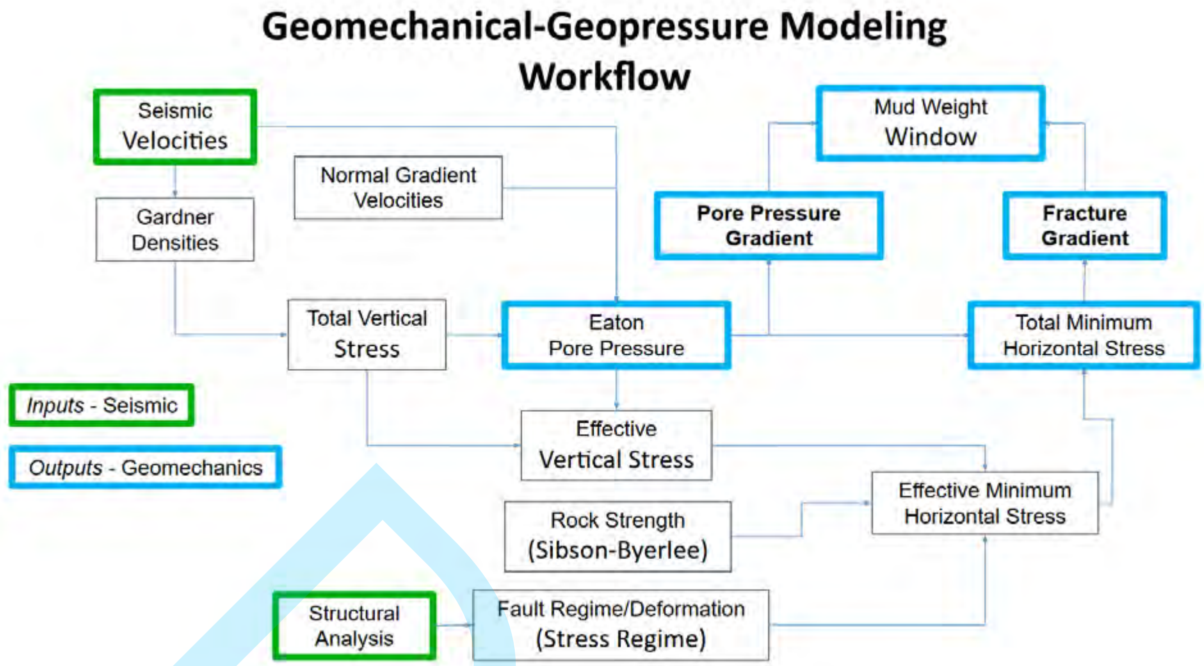

Figure 4: Detailed workflow for geomechanical and geopressure modeling from seismic velocities and structural analysis.

1974) and Eaton (Eaton, 1975) to estimate the stresses and the pore pressure. Pressure data from well 1-BRSA-61-RSS (see blue seismic line in Fig. 1) was used to compare and evaluate the pore pressure estimated according to the proposed workflow.

Petroleum system geomechanics

The last task of the proposed workflow is the analysis of geomechanical and geopressure models implications for the petroleum system of the studied area. The seal capacity and some geopressure mechanisms of petroleum systems, such as hydrocarbon generation and migration, are directly linked to the properties estimated by the geomechanical modeling (Dutta et al., 2021).

As the seismic processing is running in parallel with the proposed workflow, it is possible to check and to improve data processing results (seismic velocities, seismic images) in real time. In this way, it is possible to test and confirm the models developed and the main conclusions.

VELOCITY ANALYSIS RESULTS

The results of velocity analysis are exemplified with the seismic line 034-RL-0010 (Fig. 5). The V_{NMO} analysis of the studied CMPs is shown in Figure 6a. The *Semblance* (energy) velocity trends are clear and consistent in all 3 CMPs. Overall flattening of reflection hyperbolas in NMO corrected CMP gathers indicates the good quality of V_{NMO} picks, which means that those velocities are reliable both for depth imaging, and for quantitative seismic interpretations.

Following V_{NMO} analysis and stacking of the time domain section, the next procedure is pre-stack imaging, both in time and depth domains. Depth imaging demands interval velocities in depth domain for pre-stack

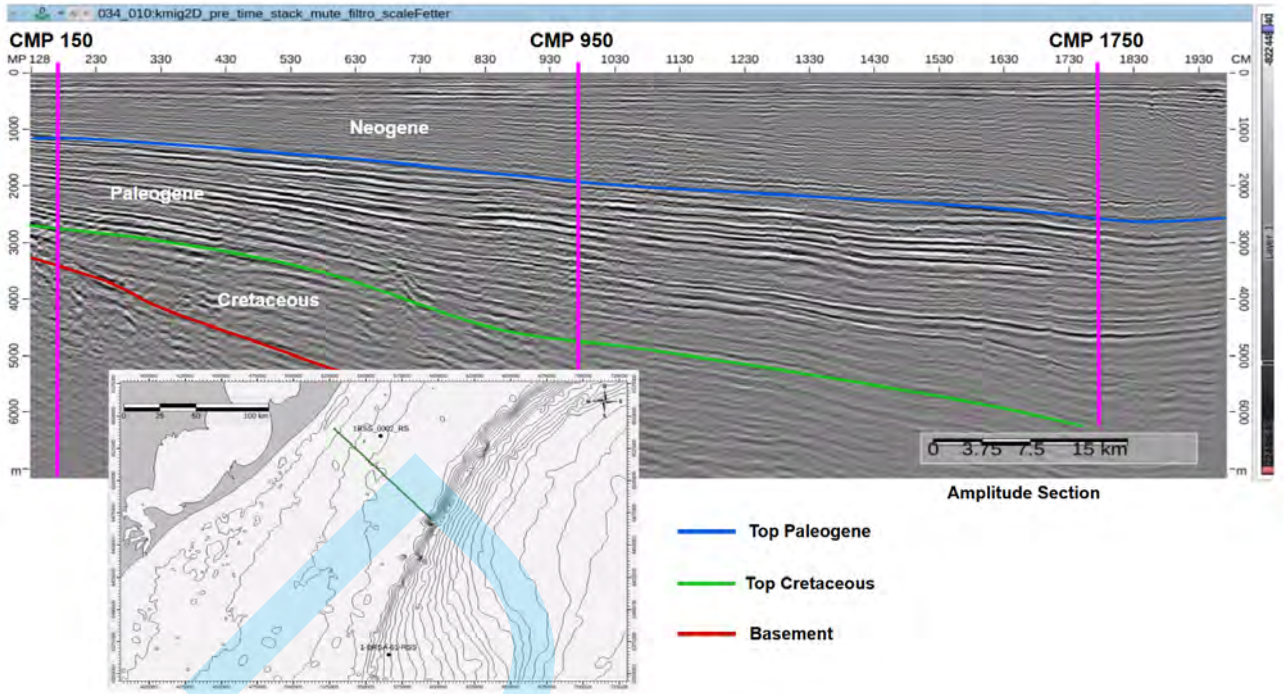

Figure 5: Depth converted seismic line 034-RL-0010 (Amplitude section), oriented to NW-SE (NW on the left; 3X vertical exaggeration). The vertical magenta lines indicate the position of the CMPs that exemplify the velocity analysis procedure. The CMP 150 position is close to the coast; the CMP 950 is located at middle shelf; the CMP 1750 is positioned close to the shelf edge. The insert shows the position of the seismic line close to the shelf edge of the Pelotas Basin (green seismic line); the wells in the insert map are the same as in Fig. 1.

depth migration (PSDM). Instead of a standard DIX equation, we used a technique called Constrained (Dix) Velocity Inversion - CVI (Koren and Ravve, 2006), which defines smooth continuous V_{INT} functions, proper for Kirchhoff PSDM.

In Figure 6b we show the CVI results obtained for the studied CMPs, with the respective image gathers after Kirchhoff PSDM. Once again it is possible to observe an overall flattening of reflection events in PSDM image gathers, confirming, with a more sophisticated algorithm, the good quality of velocity analysis.

Interval velocities could be further improved with other inversion techniques and tomography. In the present study, as the structure pattern of this part of the Pelotas Basin is quite smooth, these efforts were not compensated for. CVI results proved to be reliable enough to be used for quantitative seismic interpretation in subsequent steps of the workflow.

STRUCTURAL INTERPRETATION RESULTS

The seismic line 228-RL-0315 (Fig. 7A) shows the calibration of the stratigraphic framework with the seismic data, based on the gamma-ray log at well 1-RSS-0002-RS. The **structural analysis** indicated that the deformation is not intense but is very clear and consistent throughout the studied area. In addition, the deformation pattern also has a clear control by the mechanical stratigraphy.

The **deformation analysis** is exemplified in the 228-RL-0315 seismic line (Fig. 7) and indicates that the Neogene successions above the Top Paleogene (blue horizon) are deformed by a **pervasive system of planar normal faults** (Fig. 7b), which defines an irregular seismic facies. Some faults are cutting up close to the Sea

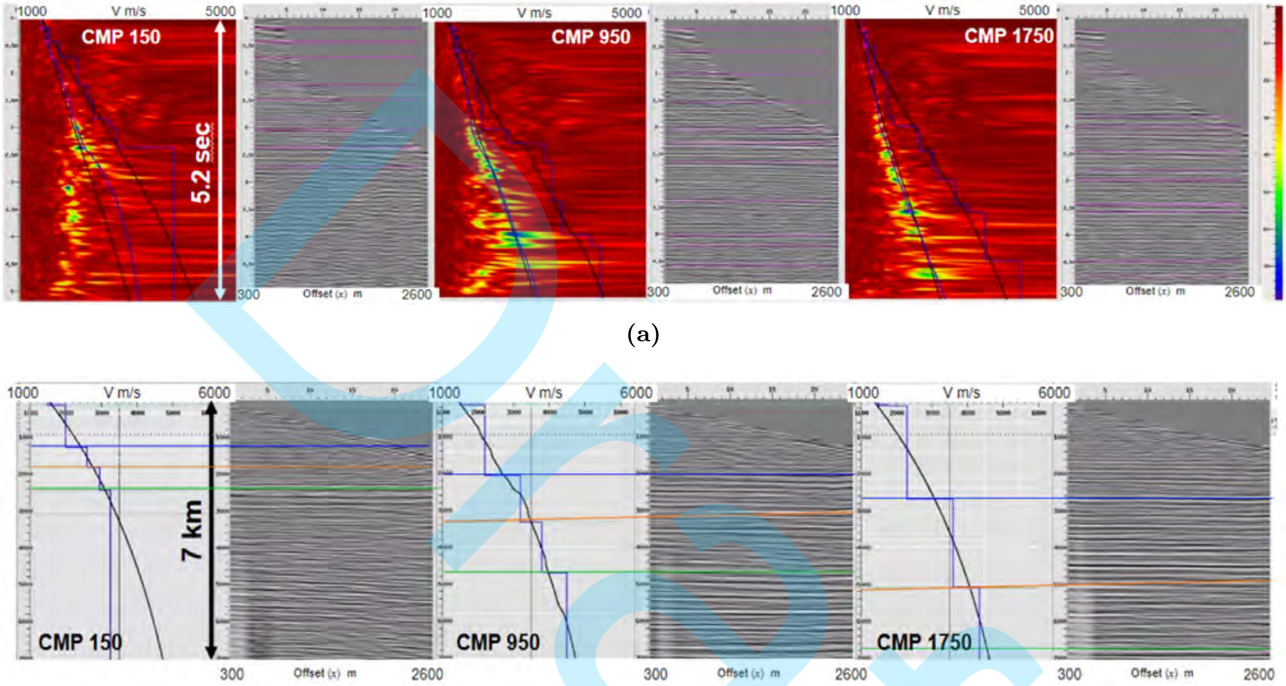

(a)

(b)

Figure 6: Results of velocity analysis in the line 034-RL-0010 (in Fig. 5, the magenta traces indicate the position of analyzed CMPs). (a) V_{NMO} results showing semblance plots and NMO corrected gathers of studied CMPs. Color scale on the right refers to semblance energy. The V_{NMO} picks on each CMP semblance plot, following semblance intensity, are on the left, and the correspondent DIX V_{INT} step functions are on the right. Observe the consistent flattening of reflection hyperbolas in NMO corrected gathers. (b) CVI results of the studied CMPs with the respective PSDM image gathers (on the right). Once again, now in the image gathers, it is clear the consistent flattening of reflection hyperbolas, obtained with pre-stack Kirchhoff depth migration. Interpreted horizons in PSDM gathers follow the stratigraphic framework of Pelotas Basin (Fig. 2). In the velocity plots (on the left) are shown the CVI continuous functions (black), and the DIX interval velocity according to the stratigraphic framework (step functions in blue).

Bottom, suggesting that deformation is related to neotectonics. Most of the faults stop down at the base of the Neogene, suggesting also the dependence on mechanical stratigraphy, as Paleogene successions are not faulted, defining a smooth seismic facies below the blue horizon (Fig. 7b).

The structural pattern shown in Fig. 7, with two seismic facies (above and below the Top Paleogene horizon), was observed in many other lines crossing the shelf edge along the studied area (Figs. 8 and 9), indicating that the described deformation is related to regional processes. Individual fault correlations are quite difficult in the 2D seismic mesh, but the interpreted fault system is possibly oriented to N30-40E, roughly parallel to the trend of the shelf border. A conceptual model based on a combination of spreading stress and flexural stress (Stein et al., 1989) fits quite well with the observed **normal fault system** (Fig. 10). The spreading stress is related to the morphology of the shelf-slope system, and the flexural stress is a response to the load of the sedimentary wedge of the Rio Grande Fan deposited beyond the shelf edge (Fig. 10; see also the **RGF** in Fig. 1). The Top Paleogene horizon acts as a neutral detachment surface which allows the reduction of the minimum horizontal stress (σ_h) in the above Neogene section to the point that produces a differential stress sufficient to cause the observed deformation pattern; below the detachment there is no such reduction of σ_h, there is not enough differential stress, and there is no deformation (Figs. 7b, 8 and 9).

GEOMECHANICAL AND GEOPRESSURE MODELING RESULTS

As indicated before, there was a great effort in this project to get reliable velocity models for stacking and depth imaging of legacy seismic data in the Pelotas Basin. With these models, we proceeded, according the proposed workflow (Fig. 4), to compute stresses and pore pressures in the same 3 selected CMPs of the studied line (Fig. 5). The objective was to test standard geomechanical equations with good quality velocity data (Fig. 6). The first parameter computed from the geomechanical model was the total vertical stress (σ_V), which can be obtained by integrating the vertical density function in each CMP (Eq. 3). The density functions were calculated from seismic velocities with Equation 4, the standard Gardner formula (Gardner et al., 1974).

$$\sigma_V(z) = \int_z \rho(z) * g * dz \tag{3}$$

$\sigma_V - total\ vertical\ stress\ (1\ MPa = 145\ psi)$

$g - gravity\ acceleration\ (9.8\ m/s^2)$

$\rho - vertical\ density\ function\ (kg/m^3)$

$$\rho(z) = 310 * V_P(z)^{0.25} \tag{4}$$

$V_P - vertical\ V_{INT}\ function\ (m/s)$

The second parameter of the geomechanical model, the pore pressure, was computed with the Eaton formula (Eq. 5), based on the ratio between observed velocities and normal gradient velocities (Eaton, 1975). Normal gradient velocities were computed through Equation 6, which was developed from shale compaction studies, and adapted to offshore basins (Pennebaker, 1968; Sayers, 2006; Dutta et al., 2021).

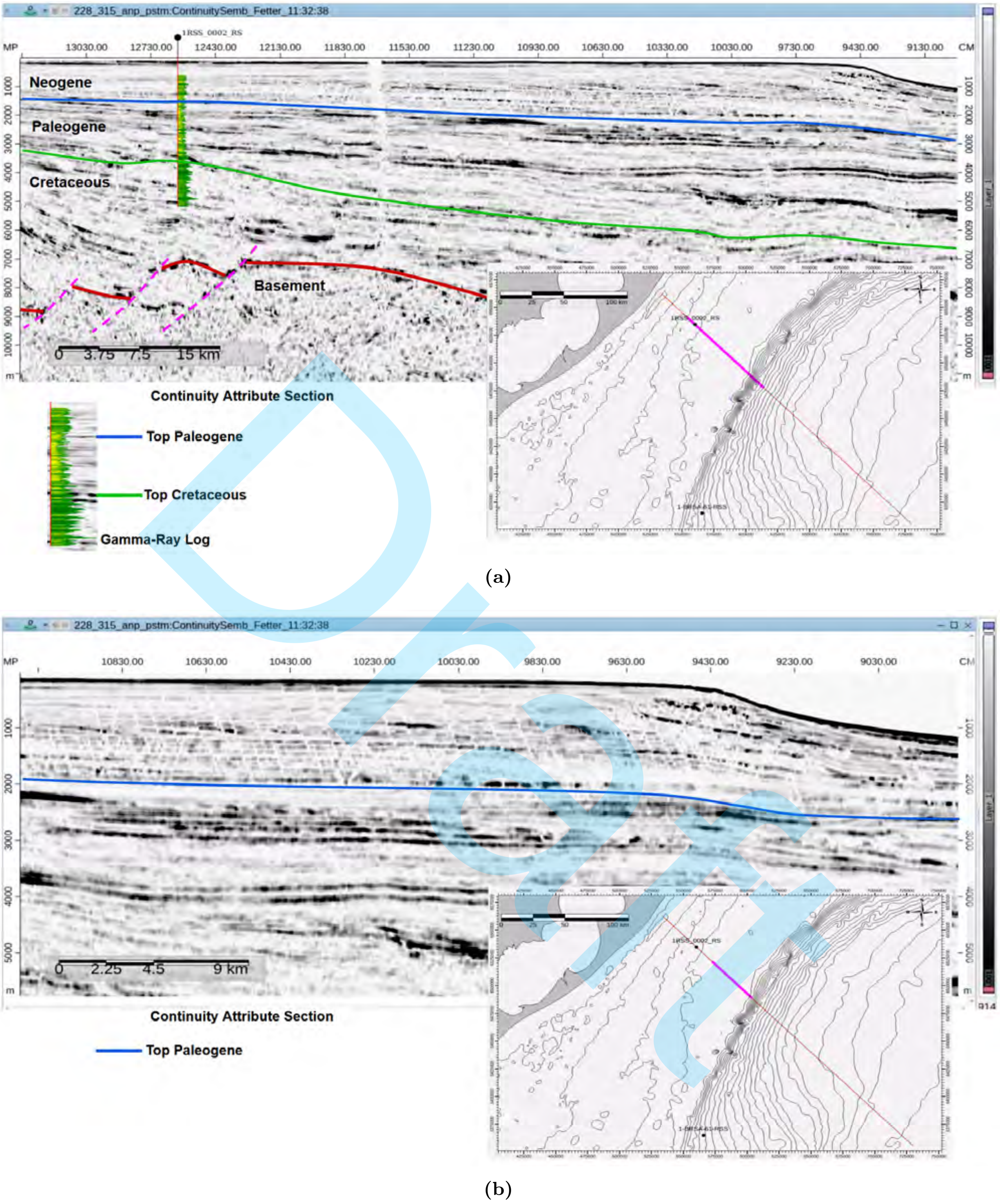

Figure 7: (a) Depth converted seismic section of the line 228-RL-0315 (*Continuity* seismic attribute) showing the calibration of the stratigraphic framework (Fig. 2) with the seismic data, based on the gamma-ray well log at well 1-RSS-0002-RS. (b) Detail of the seismic section showing deformation of Neogene sedimentary successions (above blue horizon - Top Paleogene) by a system of planar normal faults. Observe that the Paleogene successions are less deformed, as most of the faults stop down at the Top Paleogene horizon. The above described deformation pattern defines two distinct seismic facies above and below the blue horizon. The inserts show the position of the seismic line close to the shelf edge of the Pelotas Basin (thin orange line), and the specific segments of the seismic line showed in the figures (a) and (b) (thick magenta segments). Seismic sections are oriented to NW-SE (NW on the left; 3X vertical exaggeration); the wells in the insert maps are the same as in Fig. 1.

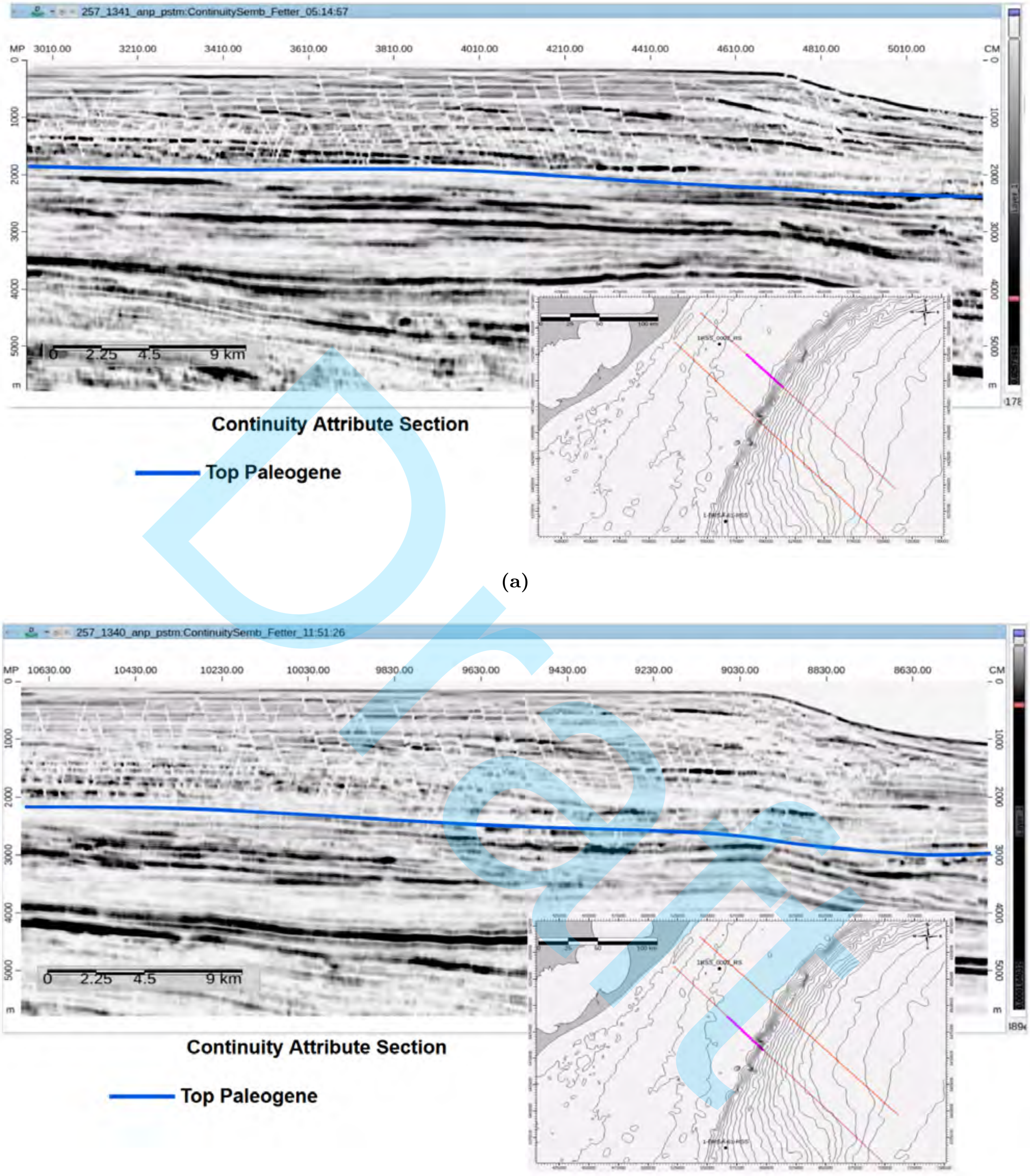

(a)

(b)

Figure 8: (a) Depth converted seismic section of the line 257-RL-1341 (*Continuity* seismic attribute). (b) Depth converted seismic section of the line 257-RL-1340 (*Continuity* seismic attribute). Both lines show the deformation pattern of Neogene sedimentary successions (above blue horizon - Top Paleogene) by a system of planar normal faults that cut up close to the Sea Bottom horizon. Observe that the Paleogene successions are less deformed, as most of the faults stop down at the Top Paleogene horizon. The interpreted deformation pattern defines two distinct seismic facies above and below the blue horizon. The inserts show the position of the seismic lines crossing the shelf edge of the Pelotas Basin (thin orange lines), and the specific segments of the seismic lines showed in the figures **a** and **b** (thick magenta segments). Seismic sections are oriented to NW-SE (NW on the left; 3X vertical exaggeration); the wells in the insert maps are the same as in Fig. 1.

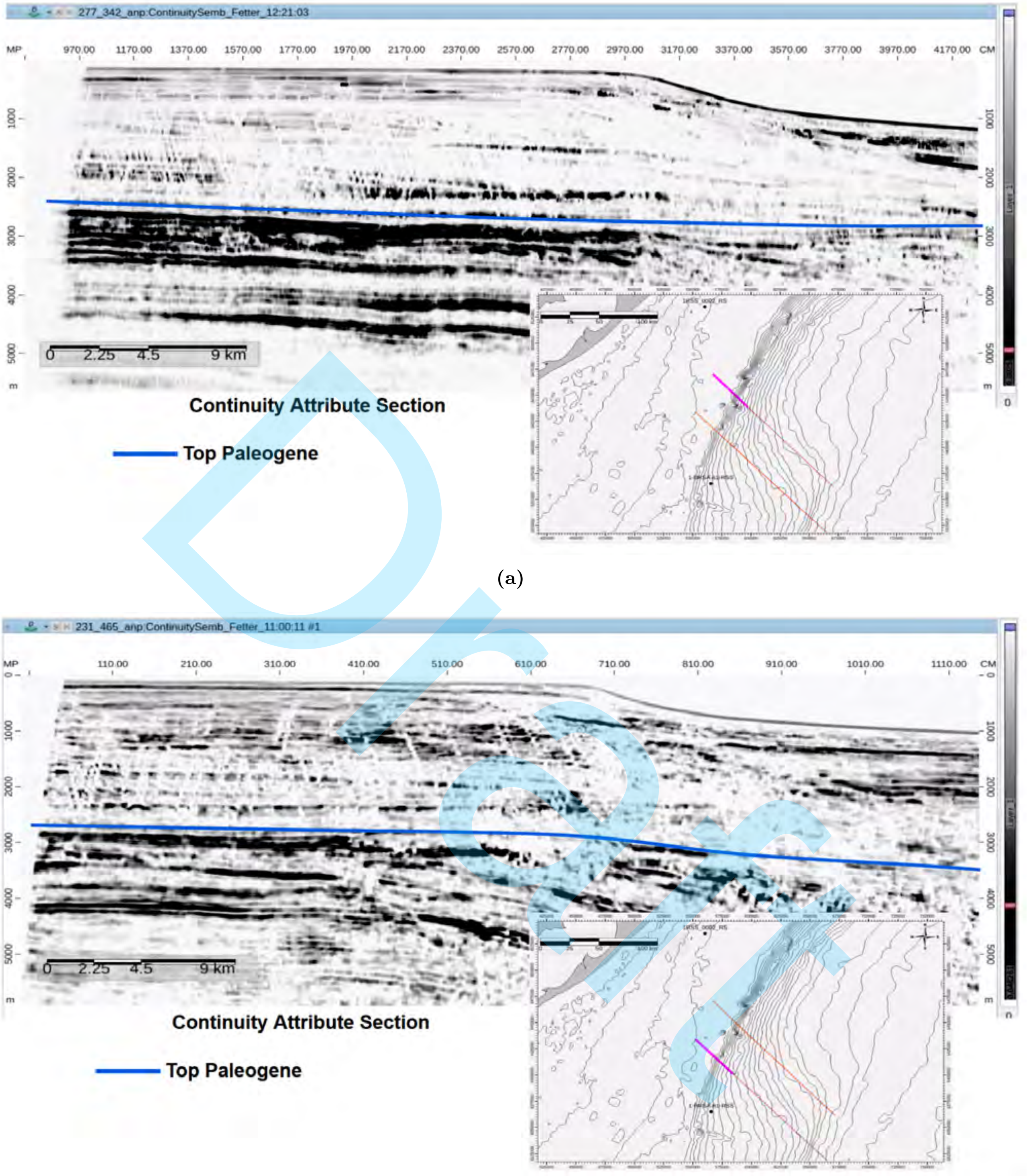

(a)

(b)

Figure 9: (a) Depth converted seismic section of the line 277-RL-0342 (*Continuity* seismic attribute). (b) Depth converted seismic section of the line 231-RL-0465 (*Continuity* seismic attribute). Both lines show the deformation pattern of Neogene sedimentary successions (above blue horizon - Top Paleogene) by a system of planar normal faults that cut up close to the Sea Bottom horizon. Observe that the Paleogene successions are less deformed, as most of the faults stop down at the Top Paleogene horizon. The above described deformation pattern defines two distinct seismic facies separated by the blue horizon. The inserts in (a) and (b) show the position of the seismic lines passing through the shelf edge of the Pelotas Basin (thin orange lines), and the specific segments of the seismic lines (thick magenta segments). Seismic sections are oriented to NW-SE (NW on the left; 3X vertical exaggeration); the wells in the insert maps are the same as in Fig. 1.

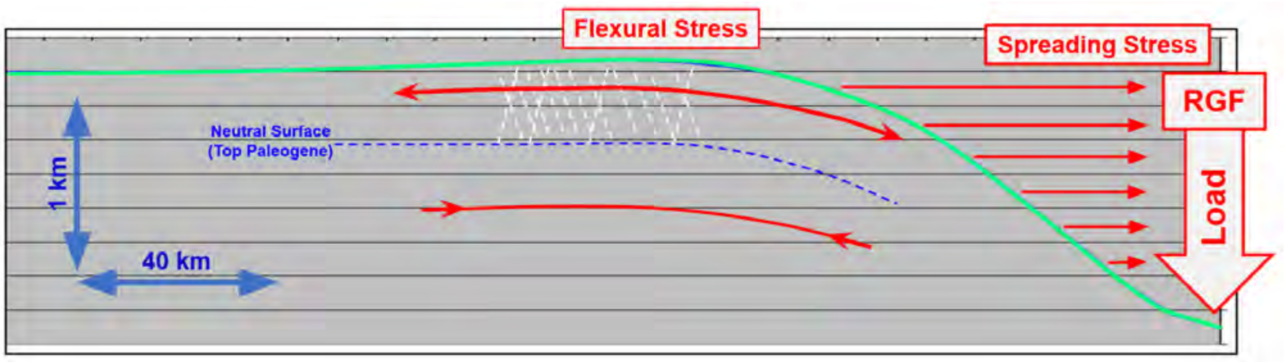

Figure 10: Conceptual model of the **normal fault system** that deforms the Neogene successions along Pelotas Basin shelf edge (thin white dashed lines). The model is based on spreading stress and flexural stress (Stein et al., 1989), active above an interpreted neutral surface at the Top Paleogene horizon. The spreading stress is related to the uncompensated load associated with the morphology of the shelf-slope system. The flexural stress is caused by the weight of the sedimentary wedge of the Rio Grande Fan (**RGF**). The neutral surface act as a mechanical detachment for the Neogene section allowing the necessary reduction of minimum horizontal stress (σ_h) for pervasive deformation in the Neogene sedimentary section. Below the detachment, in the successions of the Paleogene and the Cretaceous there is no such reduction of σ_h, and not enough differential stress to trigger deformation. The conceptual model represent the deformation pattern interpreted in Figs. 7, 8 and 9. Observe the huge vertical exaggeration used to better explain the model.

$$P_p(z) = \sigma_V(z) - (\sigma_V(z) - P_{hydro}(z)) * (V_P(z)/V_{NGrad}(z))^3 \tag{5}$$

$P_p - porepressure\ (geopressure)\ (1\ MPa = 145\ psi)$

$P_{hydro} = \int_z \rho_{hydro} * g * dz\ (1\ MPa = 145\ psi)$

$\rho_{hydro} = 1000\ (kg/m^3);\ g - gravity\ acceleration$

$V_{NGrad} - velocity\ function\ (m/s)\ calculated\ with\ normal\ gradient\ (0.6)$

$$V_{NGrad}(z) = 1500 + 0.6 * z \tag{6}$$

Comparing interpreted velocities with normal gradient velocities at the studied CMPs (Fig. 11; see CMP locations along the studied line in Fig. 5) it is possible to observe that the velocities coincide almost precisely in the proximal domain (CMP 150 - Fig. 11a), and in shallower sedimentary section, particularly in the Neogene successions (CMPs 950 and 1750 - Figs. 11b and 11c). On the other hand, in the distal domain, and in the Paleogene and Cretaceous successions, interpreted velocities are systematically lower than normal gradient velocities (CMPs 950 and 1750 - Figs. 11b and 11c). This velocity pattern suggests a hydrostatic pressure regime in proximal domain, and in the Neogene sedimentary section, and an anomalous high pore pressure regime in deeper successions, particularly in the Cretaceous section. It is important to point out that in middle shelf and shelf border the suggested hydrostatic pore pressure regime in the Neogene section is coherently coincident with the active deformation pattern indicated by structural analysis (see pervasive planar fault system in Figs. 7, 8 and 9). Besides, in proximal domain, the hydrostatic regime is probably related also with the porosity associated with the higher average sand content of the shelf sedimentary facies (Figs. 11a and 11b).

With **total vertical stresses** (Eq. 3) and **pore pressures** (Eq. 5) it is possible to compute **effective vertical stresses** according to Terzaghi's poroelastic model (Eq. 7). Structural analysis indicated that the active stress state in the studied area corresponds to a **normal fault regime** (Anderson, 1905). In such cases,

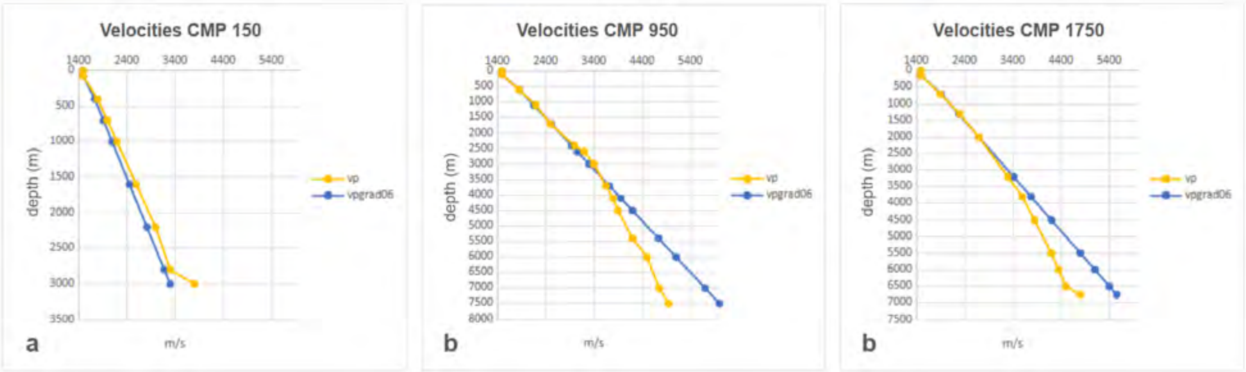

Figure 11: Interpreted velocities (vp - yellow) and normal gradient velocities V_{NGrad} (vpgrad06 - blue) for the 3 analysed CMPs along the studied line (see Fig. 5). (a) CMP 150 - **proximal domain**. Observe that the gradients are approximately equal. Interpreted velocities are slightly higher than V_{NGrad} velocities. This difference is probably related to the composition or the diagenesis of proximal sediments, with a higher average content of sand than standard shales used to compute the normal velocity gradient. (b) CMP 950 - **middle shelf domain**. Observe that the gradients are coincident in the shallower sedimentary section. Then interpreted velocities became slightly higher than V_{NGrad} velocities, again suggesting a higher average content of sand in the Paleogene successions. In the deeper Cretaceous section, interpreted velocities turn to be systematically lower than V_{NGrad} velocities, probably indicating anomalous high pore pressures. (c) CMP 1750 - **shelf border domain**. Observe that again the gradients are exactly the same in the shallower sedimentary section. Then, in deeper Paleogene and Cretaceous successions, interpreted velocities turn to be systematically lower than V_{NGrad} velocities, again suggesting anomalous high pore pressures.

brittle failure is controlled by the stress parameter R_S defined in Equation 8 (Sibson, 1974), which is the ratio between the effective vertical stress (σ'_V - maximum principal stress of the system), and the minimum effective horizontal stress (σ'_h - minimum principal stress of the system).

$$\sigma'_V(z) = \sigma_V(z) - P_p(z) \tag{7}$$

$\sigma'_V - Terzaghi's\ effective\ vertical\ stress\ (1\ MPa = 145\ psi)$

$$R_S = \sigma'_V / \sigma'_h \tag{8}$$

$R_S - Sibson's\ effective\ stress\ ratio$
$\sigma'_h - minimum\ effective\ horizontal\ stress\ (1\ MPa = 145\ psi)$

Following Sibson (1974), in brittle systems the maximum R_S stress ratio supported by a rock body depends on the Friction Coefficient (μ). It is well established in geomechanical modeling that in most sedimentary basins, we can assume a general Friction Coefficient $\mu = 0.6$ (Byerlee, 1978), which imply according to Hubbert and Willis (1957) and Sibson (1974) that, under a normal fault stress regime, a $R_S = 3$ is the maximum stress ratio supported by rock formations. In other words, for active normal fault stress regimes, the effective minimum horizontal stress σ'_h is approximately 1/3 of the effective overburden stress σ'_V.

The Stress Polygon (Zoback, 2007) is a general geomechanical model used to define possible horizontal stress states given a vertical stress value; the polygon defines the stress fields that can be supported by the average strength of the rock, according to the stress regime. In Figure 12 the Stress Polygon of the hydrostatic Neogene section is shown, with the average gradient of total vertical stress ($GradS_V = \sigma_V(z)/z = 1.10\ psi/ft$). As

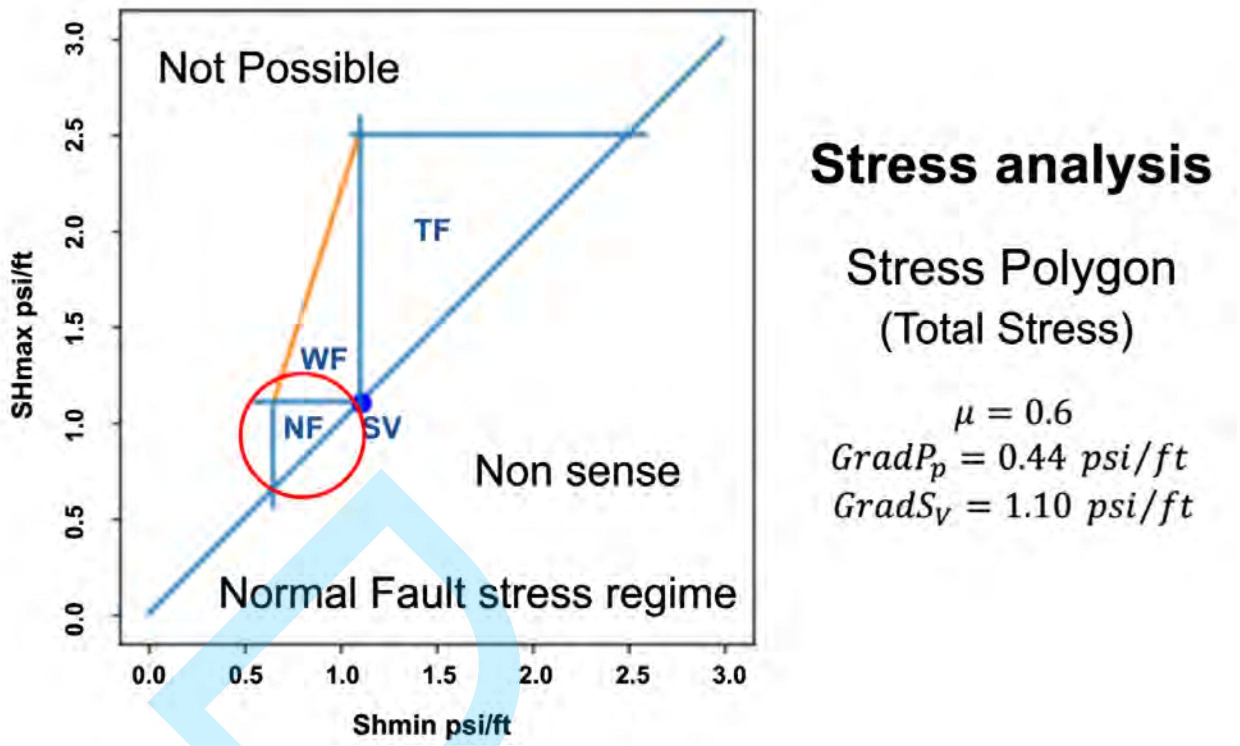

Figure 12: Stress Polygon, as defined by Zoback (2007), computed for the Neogene section with the average total vertical stress gradient ($GradS_V = \sigma_V(z)/z = 1.10\ psi/ft$),and the hydrostatic pore pressure gradient ($GradP_p = 0.44\ psi/ft$) indicated by Eaton's approach based on seismic velocities (Eq. 5; Fig. 11). The red circle indicates the field of normal fault (NF) stress regime in the studied area. The lower boundary of the gradient of minimum horizontal stress for the NF field ($S_{hmin} = 0.66\ psi/ft$) was calculated for the Friction Coefficient $\mu = 0.6$, which corresponds to a stress ratio $R_S = 3$ in terms of effective stresses. The gradient S_{hmin} is an approximation to the drilling parameter **fracture gradient**. Also indicated on the Stress Polygon are thrust fault (TF) and wrench fault (WF) stress regimes, and their boundaries for the same rock strength.

deformation is still active, the system of planar normal faults defined by structural analysis (Figs. 7, 8, 9 and 10) suggests that the lower boundary of the NF regime field on the Stress Polygon is a very good approximation for the gradient S_{hmin} (gradient of minimum total horizontal stress or **fracture gradient**) in the Neogene section (average around $S_{hmin} = 0.66\ psi/ft$; see Figure 12). This gradient is indeed equivalent to a Stress Ratio $R_S = 3$ in therms of effective stresses assuming a Friction Coefficient $\mu = 0.6$, which corresponds to a formation stressed to the limit of its strength. **Pore pressure and fracture gradients** (geopressure gradients) are important geomechanic parameters in drilling projects, as they represent, respectively, the lower and upper safe limits for mud-weight (operational window). This first general approach to a geomechanical model in the Pelotas Basin (a typical frontier exploratory area), based on the Stress Polygon, is quite reliable, and it can be obtained during seismic processing procedures, from seismic data only.

A further effort of geomechanical modeling was developed in the analysed CMPs of the studied seismic line. Departing from the pore pressure function $P_p(z)$ (Eq. 5), the **pore pressure gradient** function was computed with Equation 9, and the effective vertical stress function was computed with the Terzaghi's equation (Eq. 7). Then it was computed the effective minimum horizontal stress - $\sigma'_h(z)$, according to the mechanical stratigraphy indicated by the structural analysis. Observe that $\sigma'_h(z)$ is oriented approximately to NW-SE, perpendicular to the NE-SW trend of the mapped fault system which is probably subparallel to the shelf edge (Figs. 7, 8 and 9). For the Neogene section, which bears an active normal fault system, it was assigned a stress ratio $R_S = 3$

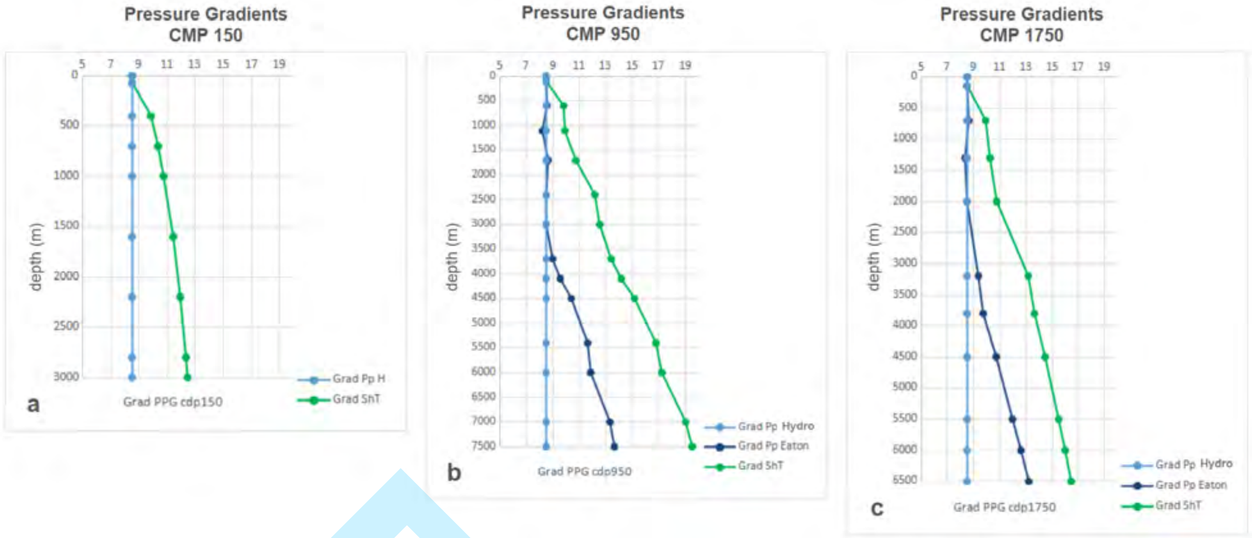

Figure 13: Hydrostatic pore pressure gradients (light blue), Eaton pore pressure gradients (dark blue), and fracture gradients (green) for the 3 analysed CMPs along the studied line (Fig. 5). (a) CMP 150 - **proximal domain**. (b) CMP 950 - **middle shelf domain**. (c) CMP 1750 - **shelf border domain**. The drilling operational window (safe mud-weight) is defined between the pore pressure gradients (blue) and the fracture gradients (green).

(assuming $\mu = 0.6$). The minimum effective horizontal stress $\sigma'_h(z)$ was calculated according to Equation 8, as 1/3 of the effective vertical stress $\sigma'_V(z)$. The same procedure was used for the Paleogene and Cretaceous successions, but with a smaller stress ratio ($R_S = 2$), as deformation analysis indicates a more stable stress state, with no active faulting (Figs. 7, 8 and 9). The function of minimum total horizontal stress was then computed just adding the functions of pore pressure and minimum effective horizontal stress (Eq. 10). Finally the **fracture gradient** was calculated with Equation 11. The geopressure gradients computed at the analyzed CMPs are shown in Figure 13.

$$GradP_p(z) = P_p(z)/z \tag{9}$$

$GradP_p - Pore\ pressure\ gradient$ ($1\ PPG$ - *pound per gallon* $= 0.052\ psi/ft$)

$$\sigma_h(z) = \sigma'_h(z) + P_p(z) \tag{10}$$

$$GradS_{hmin} = \sigma_h(z)/z \tag{11}$$

$GradS_{hmin} - Fracture\ gradient$ ($1\ PPG$ - *pound per gallon* $= 0.052\ psi/ft$)

In Figure 14 we show the results and interpretation of geomechanical modeling at CMP 1750. Hydrostatic pressure gradients calculated with the Eaton method, based on seismic velocities, coincide exactly with the Neogene section, above the Top Paleogene horizon (Chattian blue horizon), which is subjected to intense and active faulting. Just below the Neogene section, Eocene successions have a mild overpressure regime, with pore pressure gradients up to 11 PPG. Paleocene and Cretaceous successions have a more severe condition, with pore pressure gradients up to 14 PPG. In fact, in well 1-BRSA-61-RSS, located in the upper slope domain in

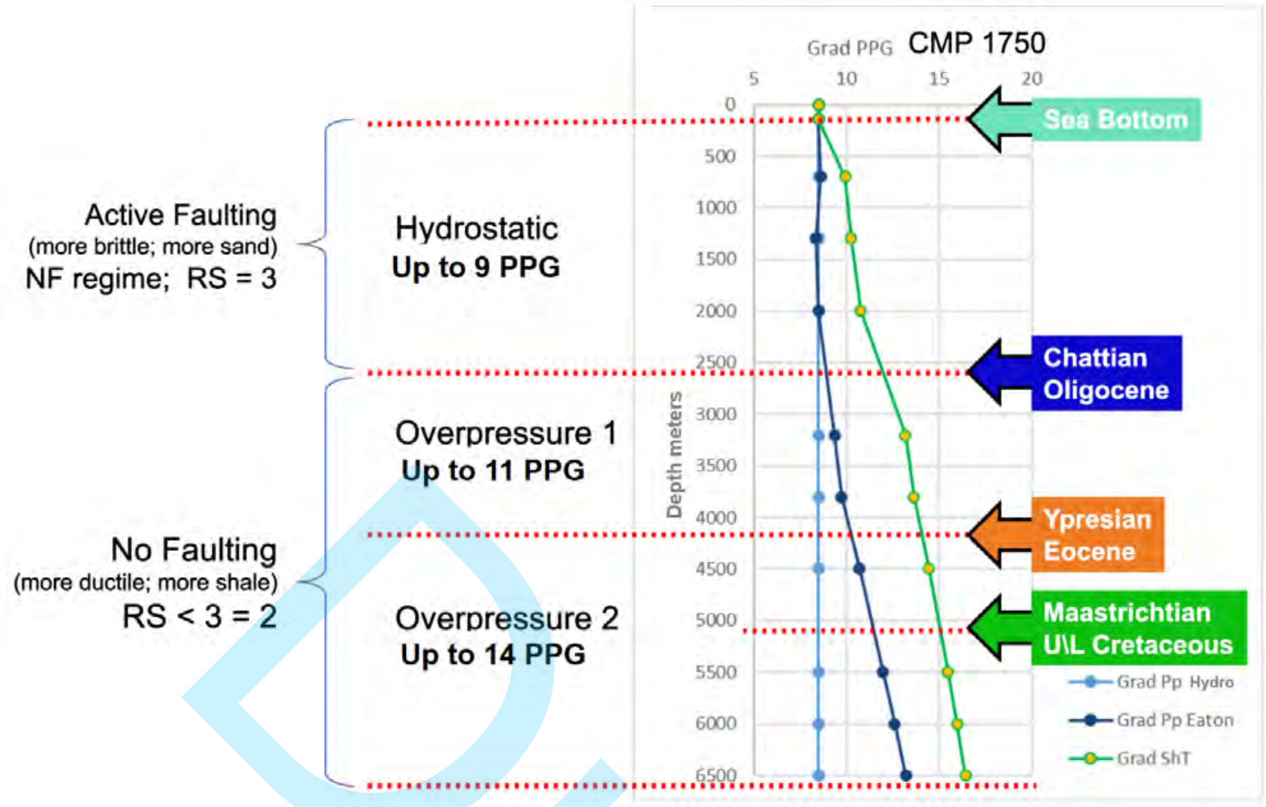

Figure 14: Pore pressure and fracture gradients in PPG (1 *pound per gallon* = 0.052 psi/ft) calculated at CMP 1750 of the studied line, at shelf border domain (see Fig. 5 for location; vertical axis is depth in meters). Light blue curve is the hydrostatic pressure gradient ($GradP_pHyd$), dark blue curve is the pressure gradient computed with the Eaton formula (Eq. 5; $GradP_pEaton$), and green curve is the fracture gradient ($GradS_hT$). Observe the stratigraphic control of pressure and fracture gradients. The window between $GradP_pEaton$ and $GradS_hT$ is a first approach to the safe mud-weight window for drilling operations in this domain of the studied area.

the eastern limit of the studied area (Fig. 15), an overpressure gradient of around 12 PPG was reported in the lower part of the Neogene successions, slightly above the gradient estimated by the model ($\approx$ 11 PPG). The well 1-BRSA-61-RSS was drilled to test a rollover structure above listric normal faults, which unfortunately disclosed only overpressure shale successions (Fig. 15). As shown before with Stress Polygon, once again deformation analysis and geomechanical modeling assembled with data available early during seismic processing can produce **coherent**, **reliable**, and **useful** results.

DISCUSSION

The results obtained so far through the integration of deformation analysis and geomechanical modeling are linked to key parameters of petroleum system analysis. Geopressure regimes are related to the sealing capacity and integrity of the system. Formations with connected pore systems, or deformed by fractures and faults, have low seal capacity and are commonly associated with hydrostatic pressures because fluids can flow easily in order to equilibrate pressure gradients. On the other hand, anomalous overpressure regimes are associated with high sealing capacity, which is also fundamental to trap hydrocarbon accumulations.

The geomechanical model of the studied area shows two different situations of the pore pressure regime

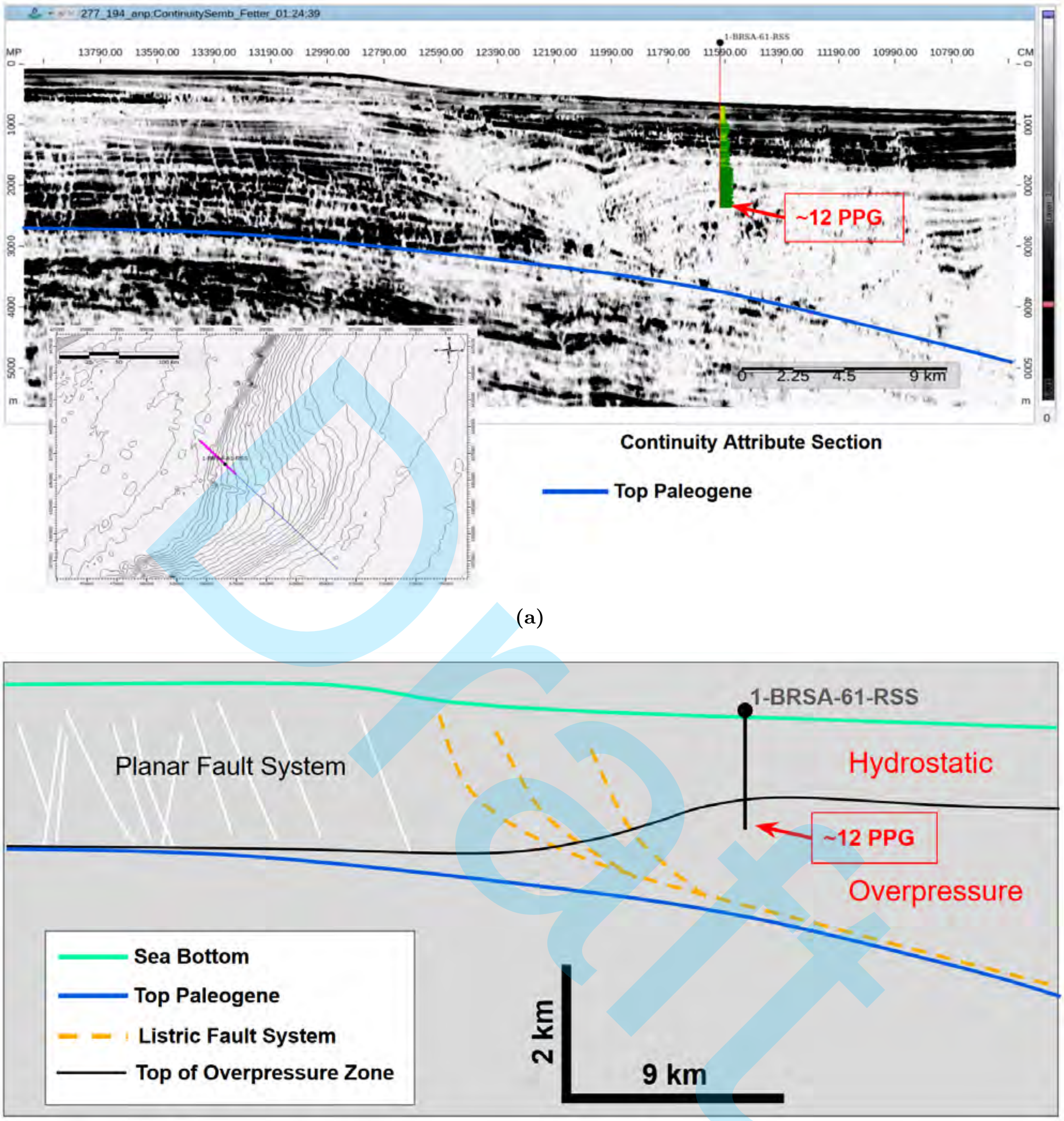

(a)

(b)

Figure 15: (a) Depth converted seismic section of the line 277-RL-0194 (*Continuity* seismic attribute). This line shows once again the deformation pattern of Neogene sedimentary successions at the shelf (above blue horizon - Top Paleogene) with a system of planar normal faults that cut up close to the Sea Bottom. The seismic line crosses the well 1-BRSA-61-RSS, which was stopped due to overpressure problems reported in the Neogene shales at the bottom of the well. The displayed log is the gamma-ray log that suggests an increase of shale content towards the base of the Neogene successions. The insert shows the position of the seismic line passing through the shelf edge in the Pelotas Basin (thin blue line), and the specific segment of the seismic line shown in the figure (thick magenta segment); the well in the insert map is the same as in Fig. 1. (b) Conceptual geopressure model considering the pore pressure estimated at the shelf border with seismic velocities ($\approx$ 11 PPG; see Fig. 14) and the pressure data observed at well 1-BRSA-61-RSS ($\approx$ 12 PPG). Seismic section and conceptual model are oriented to NW-SE (NW on the left; 3X vertical exaggeration). Well data and information reports are available at Brazilian Petroleum Agency public database (ANP).

and seal capacity (Fig. 16). The shallow proximal Neogene successions are characterized by a hydrostatic pore pressure regime, which defines a low seal capacity. In such proximal domain the observed deformation by a pervasive normal fault system improves the connection of the pore system (Figs. 10 and 16). In the distal domain, towards the shelf border and slope in deepwater environments, the Cretaceous and Paleogene deeper successions are almost certainly subject to an anomalous high pore pressure regime, considering that well data indicate overpressure even in the base of the Neogene section. Both the estimated geopressure model and the pressure data from the well reports prescribe a system with high sealing capacity and integrity in the deepwater domain in the Pelotas Basin (Fig. 16).

Seal potential defines just the boundary condition for overpressure regimes. It is important to consider also the processes that can set up overpressure in sedimentary basins. There are two basic mechanisms to engender high pore pressures: (i) to reduce pore volume of the system, trough loading or diagenesis; (ii) to increase fluid volume of the system, through aquifer inflow, thermal expansion, hydrothermal processes, diagenesis or hydrocarbon generation (Bowers, 1995, 2002). In the Pelotas Basin, the weight of the **RGF** sedimentary wedge, deposited during the Neogene, is a relevant mechanism to cause compaction and reduction of the pore volume of underlying formations (Fig. 16). The high pore pressure trend caused by subcompaction was properly calculated by the Eaton's method. The overpressure values exceeding the estimative by Eaton's method, observed at well 1-BRSA-61-RSS, suggest that the increase of fluid volume is also an important geopressure process in the studied area (Bowers, 1995). The extra load of the **RGF** brings potential source rocks of the Paleogene and Cretaceous successions into the oil and gas windows, and may also trigger water releasing by clay diagenetic transformations (Fig. 16).

CONCLUSIONS

The proposed methodology worked quite well. It is possible and recommended to bring information about geomechanics and petroleum systems during seismic processing. This procedure allows us to add value even to outdated seismic data. Besides, throughout processing, it is possible to retrieve pre-stack seismic gathers in real time, in order to check, and also to improve obtained results.

Even considering that there is only one reference well to support the results, the geomechanical/geopressure model produced out of seismic velocities is self-consistent. The hydrostatic pressure regime, defined where interpreted velocities fit normal velocity gradients, coincides thoroughly with both the proximal domain and the shallower deformed Neogene section, which have more connected pore systems.

Regarding drilling procedures in the Pelotas Basin, there is, in general, a safe operational window, but it is suggested to carefully plan the casing according to the predicted pressure regimes, because there are significant pressure variations. As overpressure gradients can be severe in deeper sedimentary successions (up to 14 PPG), it is also suggested to consider the use of Managed Pressure Drilling technology (MPD) to monitor such pressure changes.

The overpressure regime found in Cretaceous successions, based on enduring low velocity trends, points to good seal capacity, and probably to hydrocarbon generation. So, the successful Cretaceous play recently confirmed in the counterpart margin of the South Atlantic, in Namibia, may also occur in the Pelotas Basin.

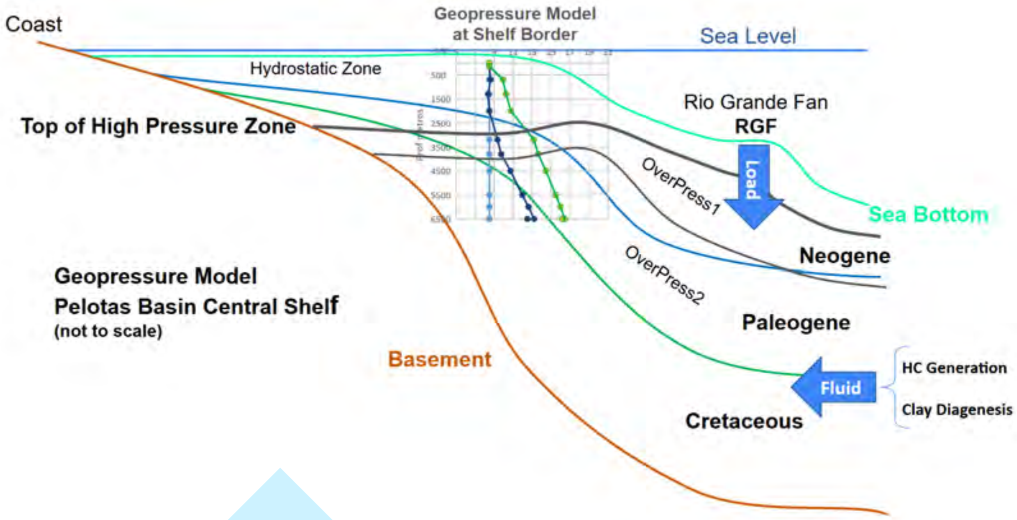

Figure 16: Geologic section showing the conceptual geopressure model of pore pressure domains and seal properties in the studied area. The hydrostatic pressure regime indicates low seal potential in proximal domains and in the Neogene section, subjected to intense faulting. On the contrary, seal potential is certainly high in overpressure zones. The load of the **RGF** sedimentary wedge caused extra compaction, reducing the volume of pore systems in the deeper portions of the shelf, and in Cretaceous successions. Additionally, the weight of the **RGF** probably bring more fluid to the system, either through hydrocarbon generation, or clay diagenesis. Both pore volume reduction and fluid volume increase produce the observed overpressure regime (Bowers, 1995). Light green horizon is the Sea Bottom; blue horizon is the Top Paleogene; green horizon is the Top Cretaceous (see Fig. 2). Thick dark gray line is the interpreted top of the overpressure zone; thin dark gray is the top of the more severe overpressure zone (see Fig. 14). Model section is oriented to NW-SE (NW on the left; not to scale).

ACKNOWLEDGEMENTS

The authors thank **Petrobras** for funding the project (Proj. ANP 21710-9: **Determinação de Parâmetros, Registro e Processamento de Dados Sísmicos para Investigação Sismoestratigráfica em Deltas e Sistemas Costeiros**), **ANP** (Brazil's National Petroleum Agency) for providing the dataset and **Aspen Technology** for supporting the software package used for seismic interpretation. **Universidade Federal Fluminense** (UFF, Niteroi/RJ, Brazil) and **Fundaçao Euclides da Cunha** (FEC) provided administrative and logistic support.

AUTHOR CONTRIBUTIONS

Marcos Fetter: Conceptual workflow, seismic processing, structural analysis, geomechanic-geopressure modeling, writing. **Guilherme Lenz**: Conceptual workflow, dataset organization, seismic processing, geomechanic-geopressure modeling, writing. **Roberto Miyamoto Pessoa**: Seismic processing, writing. **Ursula Belem da Silva**: Seismic processing, writing. **Tais Zanato**: Seismic processing, writing. **Rodrigo Stern**: Dataset organization, seismic processing, writing. **Marco Cetale**: Project management, conceptual workflow, seismic processing, writing.

CONFLICTS OF INTEREST

The authors declare no conflict of interest.

COPYRIGHT AND OPEN ACCESS

REFERENCES

Abreu, V. S., 1998, Geologic evolution of conjugate volcanic passive margins: Pelotas Basin (Brazil) and Offshore Namibia (Africa); Implications for global sea-level changes: PhD thesis, Rice University, Houston/TX, US. (VictorAbreu PhD Thesis, Accessed Aug2025).

Anderson, E. M., 1905, The dynamics of faulting: Transactions of the Edinburgh Geological Society, **8/3**, 387–402. (https://doi.org/10.1144/transed.8.3.387).

Avseth, P., T. Mukerji, and G. Mavko, 2010, Quantitative Seismic Interpretation: Cambridge University Press. (http://www.cambridge.org/9780521151351, 359 p; Accessed Aug2025).

Blakeley, I., 2022, Venus-1X: Itroducing a new distal basin floor fan play for margins: GeoExpro, **19/2**, 76–77. (BlakeleyGeoExpro2022, Accessed Aug2025).

Bowers, G. L., 1995, Pore pressure estimation from velocity data - accounting for overpressure mechanisms besides undercompaction: SPE Drilling and Completion, **June/1995**, 89–95. (https://doi.org/10.2118/27488-PA).

Bowers, G. L., 2002, Detecting high overpressure: The Leading Edge SEG, **21/2**, 174–177. (https://doi.org/10.1190/1.1452608).

Bueno, G. V., 2021, Bacia de Pelotas em retrospectiva: Contribuições à geologia do Rio Grande do Sul e de Santa Catarina, SBG Publ, 389–402. (https://doi.org/10.29327/537860.1-23).

Byerlee, J., 1978, Friction of rocks: Pure and Applied Geophysics, **116**, 615–626. (https://doi.org/10.1007/BF00876528).

Cassel, M. C., F. Chemale, M. R. Vargas, M. K. de Souza, T. J. Girelli, and G. S. de Oliveira, 2022, From the Andes and the Drake Passage to the Rio Grande Submarine Fan: Paleoclimatic and paleogeographic evidence in the Cenozoic Era from the South Atlantic – Austral Segment, Pelotas Basin: Global and Planetary Change, **213**, 103838. (https://doi.org/10.1016/j.gloplacha.2022.103838).

Dix, C. H., 1955, Seismic velocities from surface measurements: Geophysics, **20**, 68–86. (https://doi.org/10.1190/1.1438126).

Dutta, N. C., R. Bachrach, and T. Mukerji, 2021, Quantitative analisys of geopressure for geoscientists and engineers: Cambridge University Press. (https://doi.org/10.1017/9781108151726, 536 p).

Eaton, B. A., 1975, The equation for geopressure prediction from well logs: Presented at the Fall Meeting of the Society of Petroleum Engineers of AIME, OnePetro. (https://doi.org/10.2118/5544-MS).

Fontana, R. L., 1996, Geotectônica e sismoestratigrafia da Bacia de Pelotas e Plataforma de Florianópolis: PhD thesis, Universidade Federal do Rio Grande do Sul, Porto Alegre/RS, Brazil. (no link available).

Gardner, G., L. Gardner, and A. Gregory, 1974, Formation velocity and density—the diagnostic basics for stratigraphic traps: Geophysics, **39/6**, 770–780. (https://doi.org/10.1190/1.1440465).

Harkin, C., N. Kusznir, A. Roberts, G. Manatschal, and B. Horn, 2020, Origin, composition and relative timing of seaward dipping reflectors on the Pelotas rifted margin: Marine and Petroleum Geology, **114**, 104235. (https://doi.org/10.1016/j.marpetgeo.2020.104235).

Hedley, R., A. Intawong, F. Winter, and V. Sibeya, 2022, Hydrocarbon play concepts in the Orange Basin, in the light of the Venus and Graff oil discoveries: First Brake, **40**, 91–95. (https://doi.org/10.3997/1365-2397.fb2022043).

Hubbert, M. K., and D. G. Willis, 1957, Mechanics of hydraulic fracturing: Transactions of the AIME, **210/01**, 153–168. (https://doi.org/10.2118/686-G).

Koren, Z., and I. Ravve, 2006, Constrained Dix Inversion: Geophysics, **71/6**, R113–R130. (https://doi.org/10.1190/1.2348763).

Lovecchio, J. P., S. Rohais, P. Joseph, N. D. Bolatti, and V. A. Ramos, 2020, Mezosoic rifting evolution of SW Gondwana - A poly-phased, subduction-related, extensional history responsible for basin formation along the Argentinean Atlantic margin: Earth Science Reviews, **203**, 103138. (https://doi.org/10.1016/j.earscirev.2020.103138).

Miller, D. J., J. M. Ketzer, A. R. Viana, R. O. Kowsmann, A. F. M. Freire, S. G. Oreiro, A. H. Augustin, R. V. Lourega, L. F. Rodrigues, R. Heemann, A. G. Preissler, C. X. Machado, and G. F. Sbrissa, 2015, Natural gas hydrates in the Rio Grande Cone (Brazil): A new province in the western South Atlantic: Marine and Petroleum Geology, **67**, 187–196. (https://doi.org/10.1016/j.marpetgeo.2015.05.012).

Pennebaker, E., 1968, An engineering interpretation of seismic data: Presented at the Fall Meeting of the Society of Petroleum Engineers of AIME, OnePetro. (https://doi.org/10.2118/2165-MS).

Sayers, C. M., 2006, An introduction to velocity-based pore-pressure estimation: The Leading Edge, **25(12)**, 1496–1500. (https://doi.org/10.1190/1.2405335).

Sibson, R. H., 1974, Frictional constraints on thrust, wrench and normal faults: Nature, **249**, 542–544. (https://doi.org/10.1038/249542a0).

Stein, S., S. Cloetingh, N. H. Sleep, and R. Wortel, 1989, Passive margin earthquakes, stresses and rheology, *in* Earthquakes at North-Atlantic passive margins - Neotectonics and postglacial rebound: Springer, 231–259. (Stein-etal-1989, Accessed Sep2025).

Stica, J. M., P. V. Zalán, and A. L. Ferrari, 2014, The evolution of rifting on the volcanic margin of the Pelotas Basin and the contextualization of the Paraná–Etendeka LIP in the separation of Gondwana in the South Atlantic: Marine and Petroleum Geology, **50**, 1–21. (https://doi.org/10.1016/j.marpetgeo.2013.10.015).

Zoback, M. D., 2007, Reservoir Geomechanics: Cambridge University Press. (https://doi.org/10.1017/CBO9780511586477, 409 p).